

Bandstructure and optical properties of $\alpha - LiIO_3$ crystal

Yung-mau Nie

Institute of Physics, Academia Sinica, 128 Sec. 2, Academia Rd, Nankang, Taipei 115, Taiwan, R.O.C., e-mail: ymnie@phys.sinica.edu.tw

Received: 26 February 2007/ Revised version: date

Abstract The bandstructure was calculated by the full-potential linearized augmented plane wave method. The result reveals two important insights to the novel second harmonic generation (SHG) of alpha-phase lithium iodate ($\alpha - LiIO_3$) crystal: the existence of finite intra-band momentum matrix elements due to the non-inversion symmetry of the crystal illuminating the potential of the intra-band transition, and the strong covalent bonding between the *I*-atoms and the ligand *O*-atoms resulting the condition of the double-resonance. An inter-band transition scenario in SHG as $\alpha - LiIO_3$ in nano-structure is proposed. The optical properties were calculated within the theoretical framework of the time-dependent perturbation of the independent-particle model. The dielectric tensors and the refractive index were evaluated. Comparisons between the predictions and the re-

sults were made: the x-ray near edge absorption spectra; the refractive index at the static limit, and at finite frequencies. Possible factors attributing the calculation errors is discussed.

PACS 42.70.Mp, 73.20.At, 78.20.Ci

1 Introduction

The alpha-phase lithium iodate ($\alpha - LiIO_3$), in a hexagonal crystal as depicted in Fig. 1 [1,2], has been intensively studied in the past years due to its novel nonlinear optical [3], piezoelectric [4,5], and acousto-optic [5,6,7] properties. Its nonlinear optical property, especially in the second harmonic generation (SHG), always receives the attentions from the electro-optical technology, which is recently rising up due to the all-optical information processing for modern telecommunications systems. Furthermore, very recently the development of $\alpha - LiIO_3$ -based nano-structural systems for the nonlinear optical

* Present address: Computational Materials Science Center, National Institute for Materials Science, Sengen 1-2-1 Tsukuba, Ibaraki, Japan, 305-0047, Tel/Fax:+81-29-858-8003

waveguide is very promising because of the preservation for the novel nonlinear optical functions in the bulk. [8,9] In addition, the developments of photorefractive devices in real-time holography, and image processing, also urgently demand the ultraviolet photorefractive property of $\alpha - LiIO_3$ to improve resolution and storage capacity. [10] With the analogous characteristics: high refractive index, excellent optical transmittance in the visible and near-infrared region, and high dielectric constant, the newly invented room-temperature ferromagnetic semiconductor, TiO_2 in anatase structure under a Co -doping [11], has inspired the spintronic technology toward the magneto-optic and the optoelectronic applications. Thus presumably, the $\alpha - LiIO_3$ crystal should have the potential to be developed as magnetically doped reformations or a associated substrate material in the same way. In spite of this material being invented very early, the theoretical study at First-principles level on the electronic structure and the optical transition is surprisingly very limited. The resulting characters of bandstructure can further guide the searching and the tailoring of new nonlinear optical materials.

The present First-principles calculations were performed by the full-potential linearized augmented plane wave (FLAPW) method of density functional theory defined by the local density approximation (DFT-LDA). [12, 13, 14, 15, 16, 17] Testing by the f-sum rule [18, 19], the eigen-values and the momentum-matrix elements was verified to be valid to produce correct evaluations of op-

tical properties. By virtue of the analysis of the bandstructure, the insights for the intra-band and inter-band transitions of the remarkable SHG property are discovered. The near-edge states dominating the optical transition were further analyzed. The conclusion of it supplies an useful scenario in the classical dipole-oscillation framework to understand the dielectric response of the $\alpha - LiIO_3$ crystal. In order to comparing with the experimental results about the bandstructure, a simulation of the x-ray near edge absorption spectra was incorporated here.

On the calculation of optical functions, the time-dependent perturbation of independent particle model at the long-wavelength limit was applied, in which the eigen states of quasi-particle were approximated as those given by the DFT-LDA. In addition, in a non-perturbative way the time-dependent DFT, allowing for the ab-initio calculations on electron in external electromagnetic fields, also solves the analogous problem, so it is able to capture the strong dynamic effect of system illuminated in the high power. [21,20] On the other hand, the recently well-developed Berry phase method [22] can also directly simulate the macroscopic polarization at the ab-initio level to the external field effect. Due to a greater demand of the computation, so far they are more specified to the nonlinear optical simulations involved significant dynamic effect and the polarization in ferroelectric systems, respectively. However, the relation between the bandstructure information and the optical transi-

tion mechanisms, directly inspiring the tailoring the electronic structure of materials, can be feasibly accessed by the perturbation method. Hence, plenty previous works applied it to calculate the dielectric and SHG tensors of transparent insulators.[23,24,25,26,27,28,29,30,31,32,33] So far comparing with experimental results, such a method makes good agreement for the dielectric response calculations.

The present article is outlined as follows. In Sec. 2, the implementation of the FLAPW method and the formalism for the dielectric response will be illustrated. In Sec. 3, the resulting bandstructure and the dielectric functions will be exhibited. The insights for the novel SHG property and the optical transition structure will be discussed. In Sec. 4, the comparisons with the experiments on the x-ray near edge absorption spectra, the refractive index at the static limit and the finite frequency will be given therein. Finally, a brief summary will be given in Sec. 5.

2 METHODOLOGY AND FORMALISM

2.1 FLAPW Method

The modified FLAPW method, 'APW+lo' [16], was applied via the implementation of the WIEN2K code. [13, 14, 15, 16] The exchange-correlation potential functional was defined by the generalized gradient approximation (GGA) parameterized by Perdew and Wang [34]. The core and the valence states were respectively calculated

relativistically and semi-relativistically. The muffin-tin radii were set to be 1.8, 1.83, 1.6 Å for the *Li*, the *I*, and the *O*-atom, respectively. The expansions of associated Legendre polynomials for spherical harmonics of the wave function and of the non-spherical full-potential expansion were truncated at $l = 10$ and $l = 4$, respectively. The parameter RK_{max} was set to be 8.5. Additional local orbitals were added to incorporate low-lying valence states in the semi-core regime: 4*d*-states of the *I*-atoms, 2*s*-states of the *Li* and of the *O*-atoms. The lattice constants a and c at energy minimum, 5.574 and 5.259, were obtained by the parabolic fitting of bulk-modulus calculation, and the atomic coordinates: *Li*(0.0, 0.0, 0.07145); *I*(0.3333, 0.6666, 0.9991), and *O*(0.2470, 0.3422, 0.8379) at the equilibrium were determined by the calculation of ionic relaxation. Those resulting lattice parameters for the present bandstructure calculation are very similar to the x-ray diffraction [1] reported previously.

2.2 FORMALISM

In the independent particle model, the optical conductivity function σ is expressed as [35]

$$\sigma_{aa}(\omega) = \frac{2\pi}{\omega\Omega} \int \frac{d\mathbf{k}}{4\pi^3} \sum_{n,m} |p_{nm}^a|^2 \delta(\omega_n - \omega_m - \omega); \quad (1)$$

$$\delta(x) \equiv \frac{1}{\sqrt{\pi}\Gamma} e^{-\left(\frac{x}{\Gamma}\right)^2}, \quad (2)$$

where ω_n is the energy of the n -th band; Ω denotes the volume of unit cell; ω is the photon energy, and p_{nm}^a is the a -component of the momentum matrix element in the Cartesian coordinate. Herein, the subscript n (m)

symbolizes a conduction (valance) band. The δ function was defined as a smooth Gaussian distribution with the Γ of 0.35 eV. Thus, the imaginary part of dielectric tensor ε_2 can be obtained by the relation: $\varepsilon_2(\omega) = (2\pi/\omega)\sigma(\omega)$. By means of Kramers-Kronig transform, the real part ε_1 and the refractive index $n(\omega)$ can be obtained as follows

$$\varepsilon_1(\omega) = 1 + 8P \int_0^\infty \frac{\varepsilon_2(\omega')}{\omega'^2 - \omega^2} d\omega', \quad (3)$$

$$n(\omega) = \left(\frac{\sqrt{\varepsilon_1^2(\omega) + \varepsilon_2^2(\omega)} + \varepsilon_1(\omega)}{2} \right)^{1/2}. \quad (4)$$

The Brillouin-zone integration are achieved by the irreducible points of special-point sampling [36]. The convergence of the integration was tested. The error range was estimated to be at least less 0.1 percent by obtaining difference between two results given by the $12 \times 12 \times 11$ and the $23 \times 23 \times 21$ mesh, respectively.

3 RESULTS AND DISCUSSIONS

3.1 BANDSTRUCTURE

Firstly, the remarkable feature, all resulting bands within the range -6 to 0 eV always appear in a number of pairs slightly split from one degenerate state, is distinguishable in the Fig. 2. The resulting local density of state (LDOS), depicted in Fig. 3, indicates them to be derived by the $O - O$ and $I - O$ bonding. With respect to this point, according to the ' $\mathbf{k} \cdot \mathbf{p}$ ' method, the band dispersion about the Γ -point can be approximated to the

second order in $\Delta \mathbf{k}$ as[37]

$$E_m(\mathbf{k} + \Delta \mathbf{k}) = E_m(\mathbf{k}) + \frac{\hbar}{m} \Delta \mathbf{k} \cdot \mathbf{p}_{mm} + \frac{\hbar^2 (\Delta \mathbf{k})^2}{2m} + \frac{\hbar^2}{m^2} \sum_{n \neq m} \frac{(\Delta \mathbf{k} \cdot \mathbf{p}_{mn})(\Delta \mathbf{k} \cdot \mathbf{p}_{nm})}{E_m(\mathbf{k}) - E_n(\mathbf{k})}. \quad (5)$$

In a state with inversion symmetry, the parity of any its physical expectation is even, so the intra-band momentum matrix element p_{mm} vanishes due to the odd parity of the momentum operator. Contrarily, in a state without the inversion symmetry, a finite p_{mm} exists for the opposite situation. The former causes the first order term in the expansion to vanish so to give a perfect parabolic band curvature; however, the later results a non-zero linear dependent energy-split added to the parabolic band. The scale of p_{mm} should be much less than the $\hbar \Delta \mathbf{k}$, deduced from the resulting energy-split appearing to be very narrow. Then such a fine structure character can be viewed as the finger-print of the structural non-inversion symmetry of the $\alpha - LiIO_3$ crystal. In fact, about the SHG the existence of finite p_{mm} subjects the intra-band transitions [28, 29], though prohibited in the optical transition, so the present work reveals the potential of this transition mechanism to generate certain contribution.

Secondly, there is a large energy-split around 10eV resulted by the covalent bonding between the I -atoms and the ligand O -atoms according to the resulting LDOS, implies an extremely strong interaction associated with the bond forming. Actually it is even greater than the magnitude of the strong on-site Coulomb repulsion U in most of transition-metal or rare-earth atoms in the per-

ovskite crystals [38,39], also widely applied as nonlinear optical materials [3]. Furthermore, the derived double-gap feature exhibited in the Fig. 2, separating the $I-O$ bonding and anti-bonding states, as well as the intervening states localized on the O -atom near the Fermi surface, naturally meets the isometric inter-band spacing condition for the double-resonance of the inter-band transition in SHG. However, the Li -atom was determined to make only little contribution to the aforementioned states.

Predictably in the nano-structure system some surplus bands were induced within the gap because of the incorporation of surface localized states. According to the double-resonance scenario of the visual hole or the visual electron mechanism [23] illustrated in Fig. 4, the original novel SHG in the bulk can be still preserved; however, those bands of surface localized states, unless they near the gap-edge, would be hard to give a significant impact. On the other hand, after all presumably the number of the bands from surface localized states is much less than that from near-edge valence states in the bulk, also make it not be a major role in SHG. Such concepts should be useful to figure out the novel nonlinear optical properties in the bulk still preserving in the nano-structured systems. [8,9]

The present calculation indicates the band gap as the type of allowed indirect transition. Based on the resulting LDOS, the permitted transition between the gap-edge bands indeed occurs within each atomic muffin-tin

sphere, according to the angular momentum and parity selection rules of the atomic spectroscopy. The obtained indirect type agrees with the previous experimental conclusion [40]. It is deduced for the sake of the directionality of the near-edge p-states tending to maximize the band dispersion at the Γ -point, and to minimize it at the zone corner.[41] The obtained gap value, 3.8 eV, is slightly less than the measured edge-onset, $\simeq 4\text{eV}$, in the absorption [42,43,40,44] and the transmission spectrum [45].

The test of the f-sum rule [18,19], $\int_0^\infty \frac{2Q}{\pi} \sigma(\omega) d\omega = \sum_i f_i = N_{eff}$, was performed to exam the obtained bandstructure and the momentum matrix elements. For the very less contribution, the d -electrons of the I -atoms should be excluded, so the effective valence electrons is 52, being compatible with the results of N_{eff} : 56.83 and 56.66 for the xx and the zz -component, respectively. This implies the obtained bandstructure and momentum matrix elements to be amenable to the following optical calculations.

3.2 DIELECTRIC RESPONSE

The resulting components of the dielectric tensor are exhibited in Fig. 5. In fact, the resulting yy -component is identity to the xx -one, consisting with the experimental observations. The significant optical anisotropy behaves as the obviously different dispersions between the xx - and the zz -component. It is actually dominated by the

discrepancy of respective strength component, $|p_{nm}^a|^2$, in the Eqn.(1). Though the information of bandstructure is hard to directly access the insight of this quantity, it still supplies the optical transition knowledge: the initial state almost localizing on the O -atoms and the final state mainly derived from the $I - O$ anti-bonding states. In fact, the absorption resonance-edge of the resulting imaginary part given by the gap separating the above two classes states, and the location of the absorption peak, 7eV, equivalent to the energy-split between them, further solidate the aforementioned state information in the transition. Taking advantage of the classically electromagnetic radiation concept, the dynamical distribution of the charge-density in transition like a dipole rapidly oscillating out of phase along the $I - O$ bond, is useful to figure out the resulting optical anisotropy. It indeed gives an isotropic radiation on the xy -plane as the calculated result.

4 COMPARISON WITH EXPERIMENTS

The resulting X-ray absorption near edge spectra of the I -atom at the L_I , and the L_{III} -edge are shown in Fig. 6. The used parameters of resolution identity to experimental values: 0.75, and 0.66 eV [46]; the inserted values of atomic natural widths are 3.46, and 3.08 eV [47] for the L_I - and the L_{III} -edge, respectively. The present calculation agrees well with the previous measurements and their associated calculations of the multiple scattering theory [46], especially in the near edge regime. Such as

the experimentally observed white line feature at the L_I -edge, as well as the previously discovered pre-edge structure at the L_{III} -edge were reproduced. However, the discrepancy at the L_I -edge might be due to the resulting $5p$ -hybridization to be under-estimated.

The resulting refractive indices and the corresponding experimental results are listed in Table 1. In fact, the adopted formula all are approximated at the long-wavelength limit, so the most adequate comparison to the experimental data, to drastically rule out the local field and the dynamic effects, should be right at the static limit. The constant, measured from a number of independent experiments [48,49,50], is reproducible in the current calculation. Besides, the remarkable experimental negative birefringence of this crystal is also reproduced here. Since a slightly over-estimated ordinary and extra-ordinary component was produced here, this causes the disagreement with experimental values in the negative birefringence. Previous publications suggested the causes of discrepancy originating from the defect in details of the bandstructure [53,54], so the unincorporated non-local effect of the exact density functional [55] is deduced to make certain influence to them.

The resulting dispersion of the ordinary n_o and the extra-ordinary refractive index n_e at finite frequencies are shown in the Fig. 7. Generally, the present results perfectly match the frequency-dependent trend and give a consistent deviation with respect to the experimental measurements in the transparent regime. Some degree of

discrepancy from the experiments might be the result of un-incorporations of the aforementioned non-local effect and the dynamic many-body effect, and the local field effect.

5 SUMMARY

The truth of the bandstructure and the validity of the momentum matrix elements given by First-principles calculations are respectively verified by the comparison with the previous experimental result of X-ray absorption near edge spectra, and the test of the f-sum rule. The existence of finite intra-band momentum matrix elements due to the non-inverse symmetry of the crystal is revealed by the resulting bandstructure, which dominates the intra-band transition in SHG. In addition, the energy-split of the $I - O$ bonding results the condition of the double-resonance of the inter-band transition in SHG. The suggested scenario of the double-resonance in SHG as $\alpha - LiIO_3$ in the nano-structure is an useful reference to the tailoring of a same type of nonlinear optical systems. The present simulation, basing on the time-dependent perturbation in independent-particle model, can well capture the features of the linear dielectric response of the $\alpha - LiIO_3$ crystal. The discrepancies from the comparison with experiments are deduced from the ignored non-local effect in calculating the bandstructure, and the unincorporated many-body dynamic and local field effects in evaluating the dielectric functions.

Acknowledgements The author acknowledges Prof. Ding-sheng Wang for his advisements to start the study. The present work has been financially supported by National Science Council, R. O. C. (Project No. NSC92-2811-M-002-041 and NSC93-2811-M-001-065).

References

1. C. Svensson, J. Albertsson, R. Liminga, Å. Kvik, and S. C. Abrahams, *J. Chem. Phys.* **78**, (1983) 7343.
2. A. Rosenzweig and B. Morosin, *Acta Cryst.* **20**, (1966) 758.
3. S. Singh, *Handbook of Laser Science and Technology*, vol. **III**, edited by M. J. Weber (CRC Press, Boca Raton, FL, 1986); references therein.
4. S. Haussühl, *phys. Stat. sol.* **29**, (1968) K159.
5. A. W. Warner and D. A. Pinnow, *J. Acoust. Soc. Amer.* **47**, (1970) 791.
6. A. É. Aliev and A. Sh. Akramov, and R. R. Valetov, *Sov. Phys. Solid State* **31**, (1989) 2127.
7. V. V. Vorobev et al., *Sov. Phys. Solid State* **31**, (1989) 1670.
8. J. Teyssier, R. Le Dantec, C. Galez, Y. Mugnier, A. Vrain, J. Bouillot, and J.-C. Plenet, *Proc. SPIE* **5946**, (2005) 59460J.
9. J. Teyssier, R. Le Dantec, C. Galez, Y. Mugnier, J. Bouillot, and J.-C. Plenet, *Applied Phys. Lett.* **85**, (2004) 710.
10. For an review see *Photorefractive Materials and Their Applications*, edited by P. Günter and J. Huignard (Spring-Verlag, Berlin, 1988, 1989), Vols. I and II.
11. M. Ueda, Y. Sako, T. Tanaka, P. Devreotes, and T. Yanagida, *Science* **291**, (2001) 854.

12. O. K. Andersen, Phys. Rev. B **12**, (1975) 3060.
13. P. Blaha, K. Schwarz, and P. Herzig, Phys. Rev. Lett. **54**, (1985) 1192.
14. P. Blaha, K. Schwarz, and P. H. Dederichs, Phys. Rev. B **37**, (1988) 2792.
15. H. M. Petrilli, P. E. Blöchl, P. Blaha, and K. Schwarz, Phys. Rev. B **57**, (1998) 14690.
16. G. K. H. Madsen, P. Blaha, K. Schwarz, E. Sjöstedt, and L. Nordstrom, Phys. Rev. B **64**, (2001) 195134.
17. S. Cottenier, *Density Functional Theory and the Family of (L)APW-methods: a step-by-step introduction* (Instituut voor Kern-en Stralingsfysica, K. U. Leuven, Belgium, 2002, ISBN 90-807215-1-4).
18. M. Altarelli, D. L. Dexter, H. M. Nussenzveig, and D. Y. Smith, Phys. Rev. B **6**, (1972) 4502.
19. D. Y. Smith and E. Shiles, Phys. Rev. B **17**, (1978) 4689.
20. A. D. Corso, F. Mauri, and A. Rubio, Phys. Rev. B **53**, (1996) 15638, and references therein.
21. M. A. L. Marques and E. K. U. Gross, Annual Rev. of Phys. Chem. **55**, (2004) 427, and references therein.
22. D. Vanderbilt and R. Resta, "Quantum electrostatics of insulators: Polarization, Wannier functions, and electric fields," in *Conceptual foundations of materials properties: A standard model for calculation of ground- and excited-state properties*, S.G. Louie and M.L. Cohen, eds. (Elsevier, The Netherlands, 2006), pp. 139-163.
23. Ed Ghahramani, D. J. Moss, and J. E. Sipe, Phys. Rev. Lett. **64**, (1990) 2815.
24. J. E. Sipe and Ed Ghahramani, Phys. Rev. B **48**, (1993) 11705.
25. C. Aversa and J. E. Sipe, Phys. Rev. B **52**, (1995) 14636.
26. J. L. P. Hughes and J. E. Sipe, Phys. Rev. B **53**, (1996) 10751.
27. J. L. P. Hughes, Y. Wang and J. E. Sipe, Phys. Rev. B **55**, (1997) 13630.
28. J. E. Sipe and A. I. Shkrebtii, Phys. Rev. B **61**, (2000) 5337.
29. S. N. Rashkeev, W. R. L. Lambrecht, and B. Segall, Phys. Rev. B **57**, (1998) 3905.
30. S. Sharma, J. K. Dewhurst, and C. Ambrosch-Draxl, Phys. Rev. B **67**, (2003) 165332.
31. B. Adolph and F. Bechstedt, Phys. Rev. B **62**, (2000) 1706.
32. C.-G. Duan, J. Li, Z.-Q. Gu and D.-S. Wang, Phys. Rev. B **59**, (1999) 369.
33. C.-G. Duan, J. Li, Z.-Q. Gu and D.-S. Wang, Phys. Rev. B **60**, (1999) 9435.
34. J. P. Perdew and Y. Wang, Phys. Rev. B **46**, (1992) 12947.
35. J. Li, C.-G. Duan, Z.-Q. Gu, and D.-S. Wang, Phys. Rev. B **57**, (1998) 2222.
36. H. J. Monkhorst and J. D. Pack, Phys. Rev. B **13**, (1976) 5188.
37. M. Lax, *SYMMETRY PRINCIPLES IN SOLID STATE AND MOLECULAR PHYSICS* (Dover, New York, 2001), pp.211-215.
38. I. Solov'yev, N. Hamada, K. Terakura, Phys. Rev. B **53**, (1996) 7158.
39. B. N. Harmon, V. P. Antropov, A. I. Lichtenstein, I. V. Solov'yev, V. I. Anisimov, J. Phys. Chem. Solids **56**, (1995) 1521.
40. M. A. Gaffar, A. A. El-Fadl, J. of Phys. and Chem. of Solids **60**, (1999) 1633.

41. J. Singh, *Electronic and Optoelectronic properties of semiconductor structures*(Cambridge University Press, Cambridge, 2003).
42. L. L. Regel', Z. B. Perekalina, A. I. Baranov, B. V. Shchepetil'nikov, and N. A. Baturin, Sov. Phys. Crystallogr. **32**, (1988) 862.
43. J.-J. Xu, X.-F. Yue, and R. A. Rupp, Phys. Rev. B **54**, (1996) 16618.
44. C. Galez, Y. Mugnier, J. Bouillot and C. Rosso, Optical Materials **19**, (2002) 33.
45. F. R. Nash, J. G. Bergman, G. D. Boyd, and E. H. Turner, J. of Appl. Phys. **40**, (1969) 5201.
46. J. Goulon, C. Goulon-Ginet, A. Rogalev, V. Gotte, C. Malgrange, C. Brouder, and C. R. Natoli, J. of Chem. Phys., **108**, (1998) 6394.
47. M. O. Krause and J. H. Oliver, J. Phys. Chem. Ref. Data **8**, (1979) 329.
48. G. Nath and S. Haussuhl, Appl. Phys. Lett. **14**, (1969) 154.
49. S. Umegaki, S.-I. Tanaka, T. Uchiyama and S. Yabumoto, Opt. Commun. **3**, (1971) 244.
50. K. Takizawa, M. Okada and S. Ieiri, Opt. Commun. **23**, (1977) 279.
51. J. M. Crettez, J. Comte and E. Coquet, Opt. Commun. **6**, (1972) 26.
52. R. L. Herbst, quoted by M. M. Choy and R. L. Beyer, Phys. Rev. B **14**, (1976) 1693.
53. W. R. L. Lambrecht and B. Segall, Phys. Rev. B **40**, (1989) 7793.
54. Z. H. Levine and D. C. Allan, Phys. Rev. B **43**, (1991) 4187.

Table 1 The refractive indices of $\alpha - LiIO_3$ crystal at the static limit. The ' n_o ', the ' n_e ' and the 'B' label the ordinary, the extra-ordinary component, and the birefringence, respectively. The λ labels the operating wavelength.

Result	n_o	n_e	B	λ (nm)
Present	2.1127	1.7940	-0.3187	-
Exp1 [48]	1.8385	1.7050	-0.1275	2249.3
Exp2 [49]	1.860	1.719	-0.141	1060
Exp3 [50]	1.7940	1.6783	-0.1157	5000

55. W. G. Aulbur, L. Jönsson, and J. W. Wilkins, Phys. Rev. B **54**, (1996) 8540.

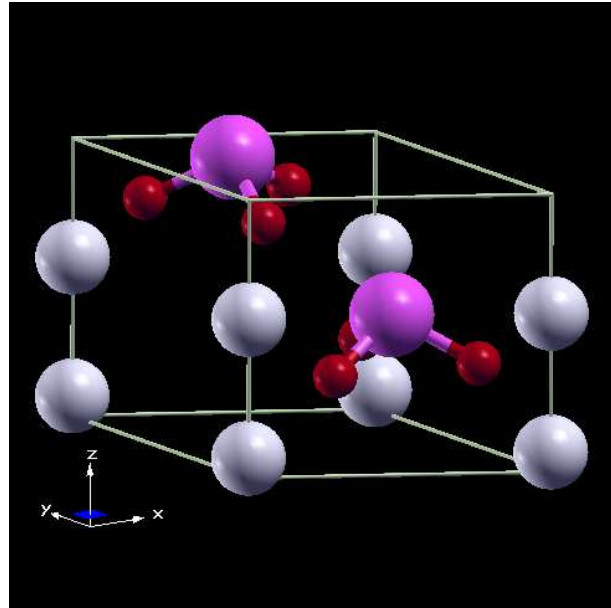


Fig. 1 The unit cell structure of the $\alpha - LiIO_3$ crystal. In the bonding sketch, each I -atom (purple color) locates at the top of pyramid based by three O -atoms (red color). The Li -atoms (grey color) reside the sites on the edge.

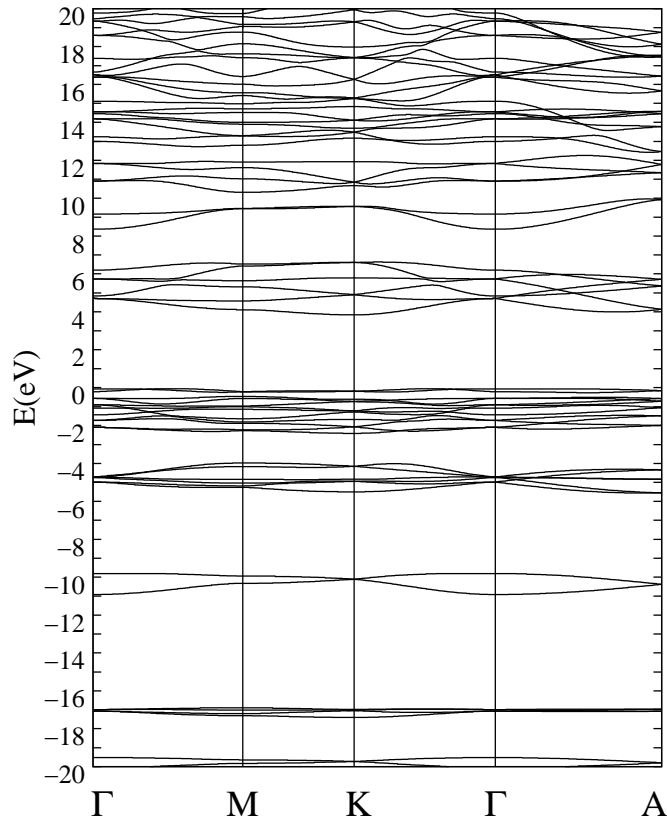


Fig. 2 The bandstructure of the $\alpha - LiIO_3$ crystal. Here $\Gamma : (0, 0, 0)$; $M : 2\pi/a(1/2, 0, 0)$; $K : 2\pi/a(1/3, 1/3, 0)$, and $A : 2\pi/c(0, 0, 1/2)$.

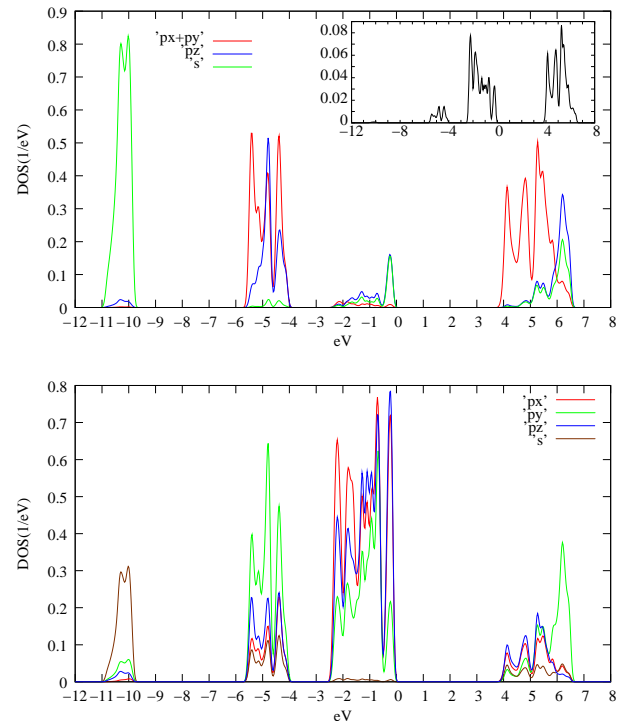


Fig. 3 The LDOS for the s- and p-states of the I -atom (top) and the O -atom (bottom). The inset of the top panel depicts the result of d-states of I -atom.

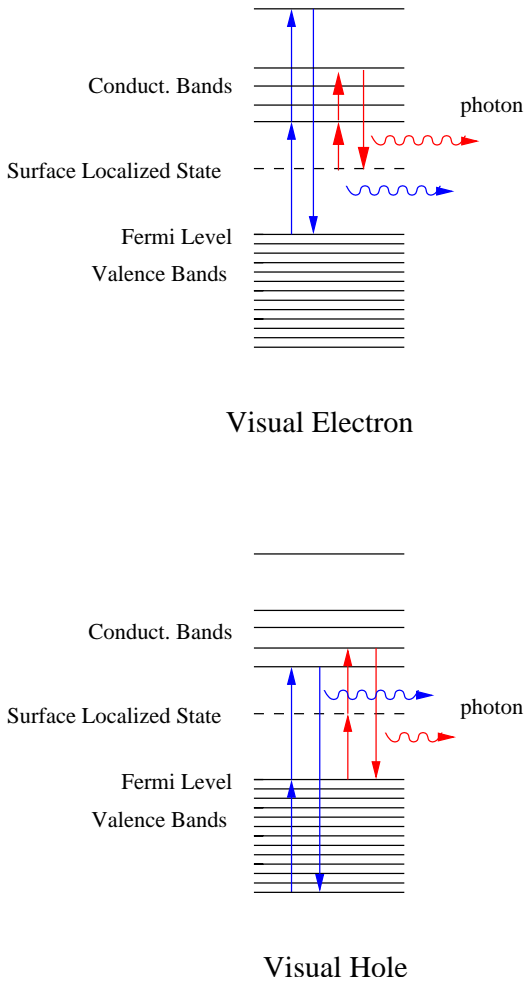


Fig. 4 The visual hole and the visual electron mechanisms of the inter-band transition in SHG. The blue arrow depicts the original transition in the bulk, and the red specifies to the case for the bands of surface localized states only.

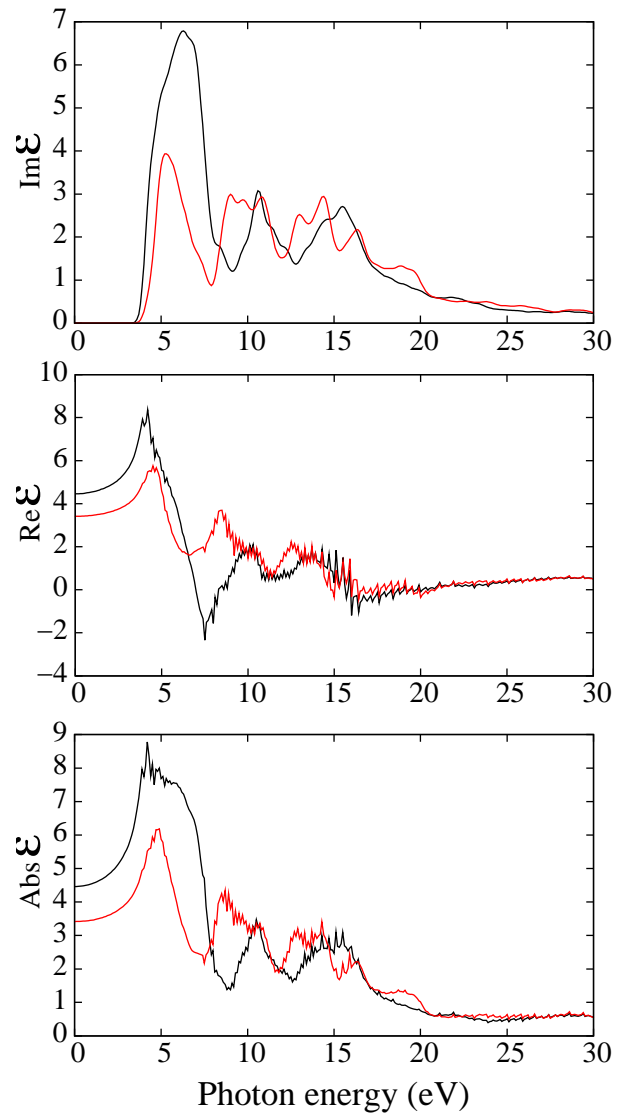


Fig. 5 The dispersion of the imaginary part, the real part, and the absolute of the dielectric tensor (in the unit of $(\text{eV} \cdot \text{sec})^{-1}$). The black and the red lines depict the ϵ_{xx} - and the ϵ_{zz} -components of the dielectric function, respectively.

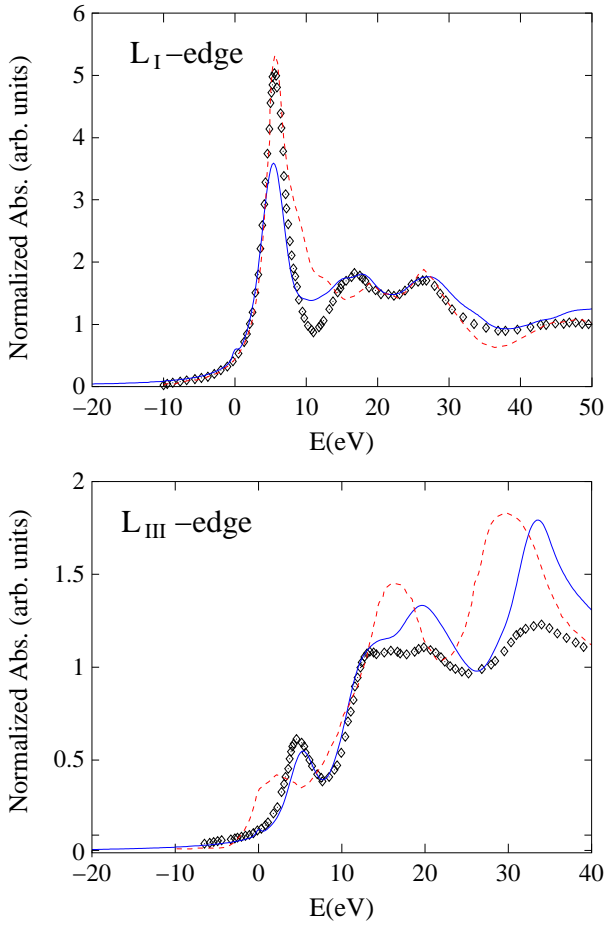


Fig. 6 The X-ray absorption near edge spectra of the I -atom at the L_I , and the L_{III} -edge. The present results, and the corresponding measurements; their associated simulations of the multiple scattering theory are respectively depicted by the blue solid line, and the diamond symbols; the red dashed line.

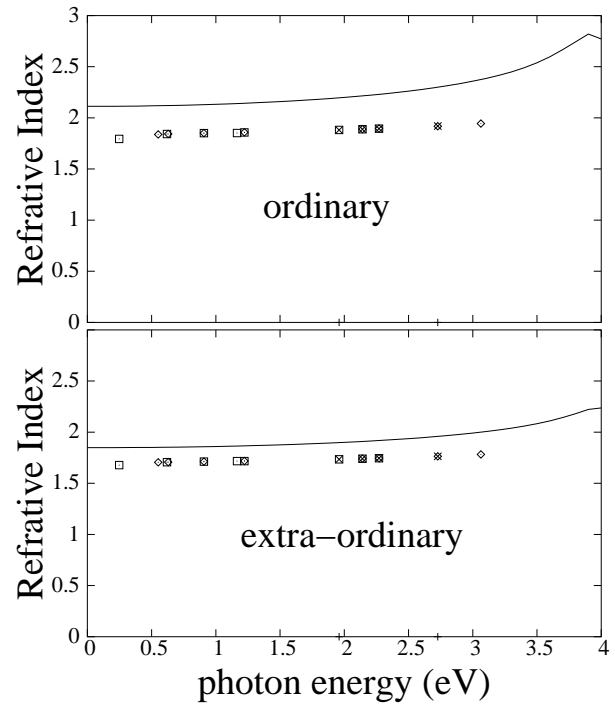


Fig. 7 The dispersion of the refractive index. The solid line depicts the present result and the diamond, the cross, the square, and the triangle symbols exhibit the measurements of references [49], [51], [52], and [50], respectively.